RSC Advances

PAPER

View Article Online
View Journal | View Issue

Cite this: *RSC Adv.*, 2025, **15**, 13214

Synthesis, molecular docking, and biological investigations of new pyrazolone chalcones†

Ahmed A. Noser, *[a] Maha M. Salem, [b] Esraa M. ElSafty,[a] Mohamed H. Baren,[a] Adel I. Selim[a] and Hamada S. A. Mandour[a]

Received 20th February 2025
Accepted 10th April 2025

DOI: 10.1039/d5ra01233c

rsc.li/rsc-advances

Heterocyclic compounds are essential to the drug development and discovery processes. Herein, we synthesized new pyrazolone chalcones (**3a–g**) through the reaction of azopyrazolone (**2**) with different aromatic aldehydes in a basic medium. Numerous techniques including elemental analysis, ^{1}H-NMR, ^{13}C-NMR, and FT-IR spectroscopies, were used to characterize pyrazolone chalcone derivatives. Compound **3b** exhibited the highest binding energy towards YAP/TEAD protein with a value of −8.45 kcal mol^{-1} in *in silico* studies. This observation suggested that compound **3b** inhibits the YAP/TEAD Hippo signaling pathway. In addition, compound **3b** offered a prospective anticancer effect against various cancer cell lines, such as HepG-2, MCF-7, and HCT-116, among the other synthesized compounds, with IC_{50} values equal to 5.03 ± 0.4, 3.92 ± 0.2, and 6.34 ± 0.5 μM, respectively. These results validated our findings regarding the *in silico* suppression of the YAP/TEAD protein. Its pharmacokinetic properties were theoretically observed using ADMET. Additionally, compound **3b** demonstrated a potent antioxidant scavenging action (*in vitro*) against DPPH free radicals. Thus, based on our findings, compound **3b** may act as a potential anticancer scaffold owing to its inhibitory impact towards the YAP/TEAD-mediated Hippo signaling pathway with a safe toxic profile on normal cells.

Introduction

Cancer is a worldwide civic health concern, and its diagnosis in early stage is of great importance.[1] Currently, the primary treatment strategies for cancer are chemotherapy, surgery, and targeted therapy. Targeted therapy has become a standard treatment for cancer patients and has significantly increased the efficacy of cancer therapy.[2] According to a previous report, regulating organ growth and inhibiting tumors depend on the Hippo signaling target pathway's control over cell division and proliferation.[3] Because of its significant influence on patient prognosis and chemotherapeutic drug resistance, the Hippo pathway is a desirable therapeutic target.[4] Pyrazoles have attracted significant attention owing to their effective pharmaceutical properties such as antibiotic, antifungal, antibacterial, pesticidal, antioxidant, anti-inflammatory, antiviral, and antitumor effects.[5–11] Chalcones are α,β-unsaturated ketones with a broad range of pharmacological actions, making them interesting synthons and bioactive scaffolds with great therapeutic potential. It is commonly known that they have significant biological effects such as antibacterial, antioxidant, and anticancer effects.[12–15] Chalcones facilitate the synthesis of novel heterocyclic compounds including pyrimidinones, azepines, pyridine, and pyran, which have strong biological activities.[16,17] There have been numerous reports on marketed anticancer drugs containing pyrazolone and a chalcone core, such as metochalcone, sofalcone, butein, metamizole, and propyphenazone,[18–22] as shown in Fig. 1.

The goal of our study was to develop a new class of pyrazolone chalcone derivatives, examine their radical scavenging activities and investigate their anticancer effects by inhibiting the YAP/TEAD Hippo signaling pathway (*in silico*). our findings confirmed their impact on cancer cell lines (*in vitro*). Additionally, absorption–distribution–metabolism–excretion–toxicity (ADMET) pharmacokinetic features were used to assess their drug-likeness and bioavailability.

Results and discussion

Chemistry of the novel compounds

Scheme 1 describes the reaction of ethyl cyanoacetate with phenyl hydrazine, which leads to the formation of compound **1**, as described previously by Weissberger.[23] Further modification of compound 1 with *p*-acetyl phenyl diazonium chloride offered azo pyrazolone **2** with 74% yield (Scheme 1). The chemical

[a]*Organic Chemistry, Chemistry Department, Faculty of Science, Tanta University, Tanta 31527, Egypt. E-mail: ahmed.nosir@science.tanta.edu.eg; esraa_elsafty@science.tanta.edu.eg; chemistnoser2010@yahoo.com; adel.saleem@science.tanta.edu.eg; hamada.mandour@science.tanta.edu.eg*

[b]*Biochemistry Division, Chemistry Department, Faculty of Science, Tanta University, Tanta 31527, Egypt. E-mail: maha_salem@science.tanta.edu.eg*

† Electronic supplementary information (ESI) available: Materials and instruments used during the synthesis and the spectral data of the new compounds. See DOI: https://doi.org/10.1039/d5ra01233c

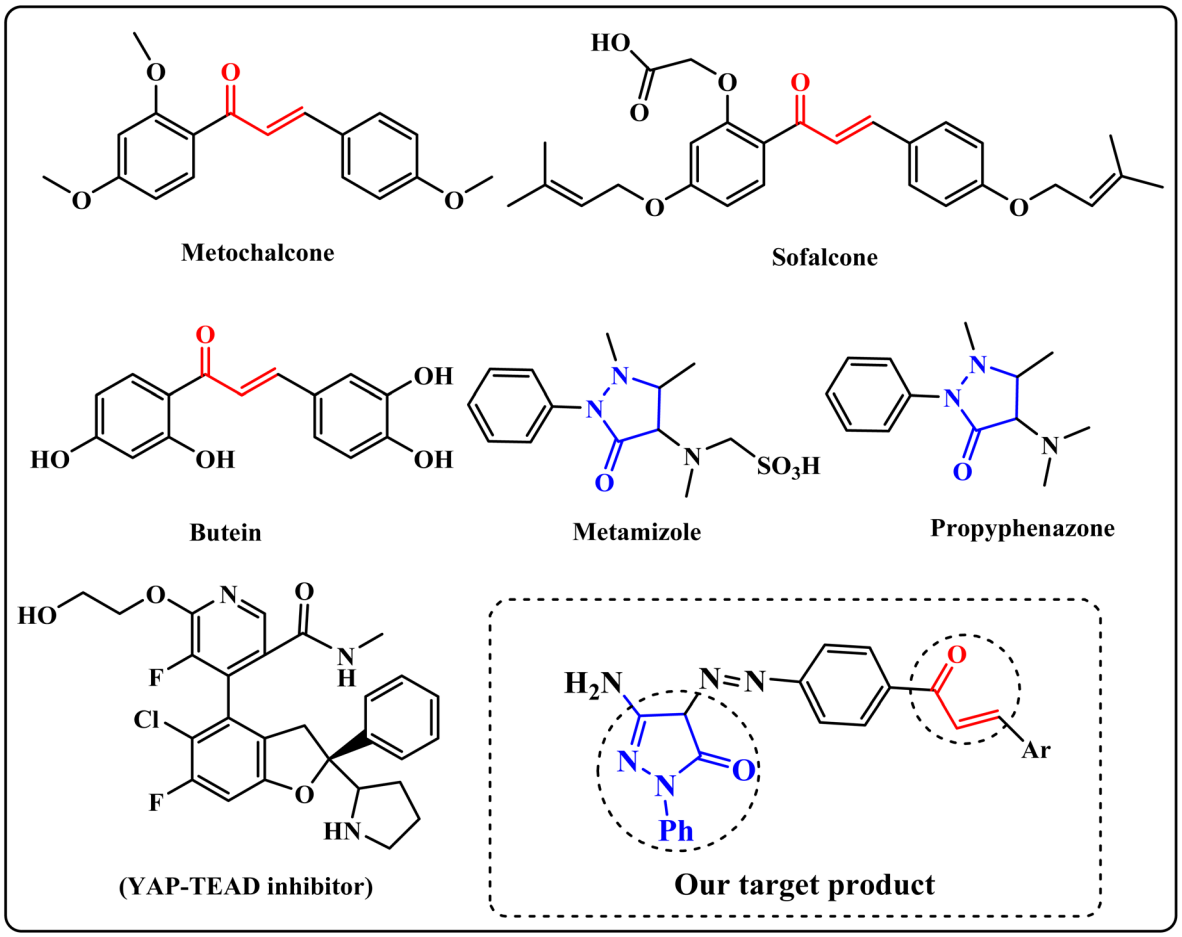

Fig. 1 Marketed pyrazolone- and chalcone-based drugs.

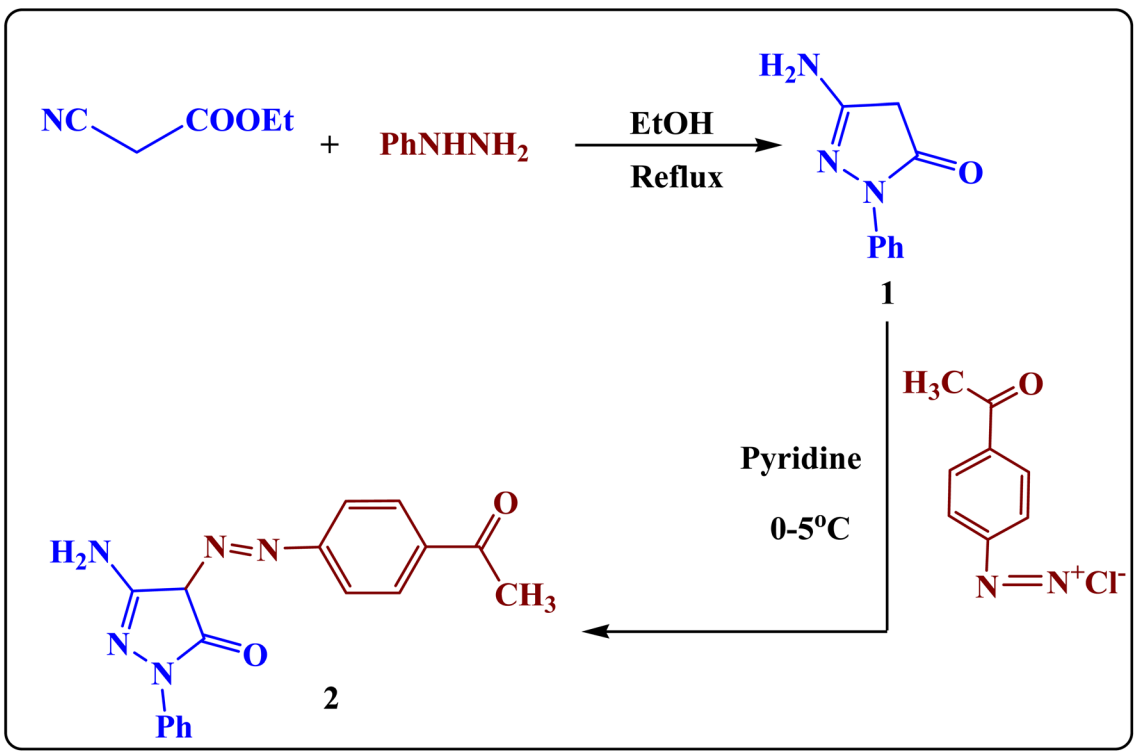

Scheme 1 Synthesis route for compound 2.

structures of compounds **3a–g** were established according to their elemental analysis and different spectral data. Elemental analysis was used to indicate the exact ratio of C, H, and N. Fourier transform infrared (FT-IR) spectroscopy was used to illustrate the presence of the main functional groups. Nuclear magnetic resonance (NMR) was used to indicate the different types of hydrogen and carbon atoms in the synthesized compounds. The FT-IR analysis of compound **2** showed

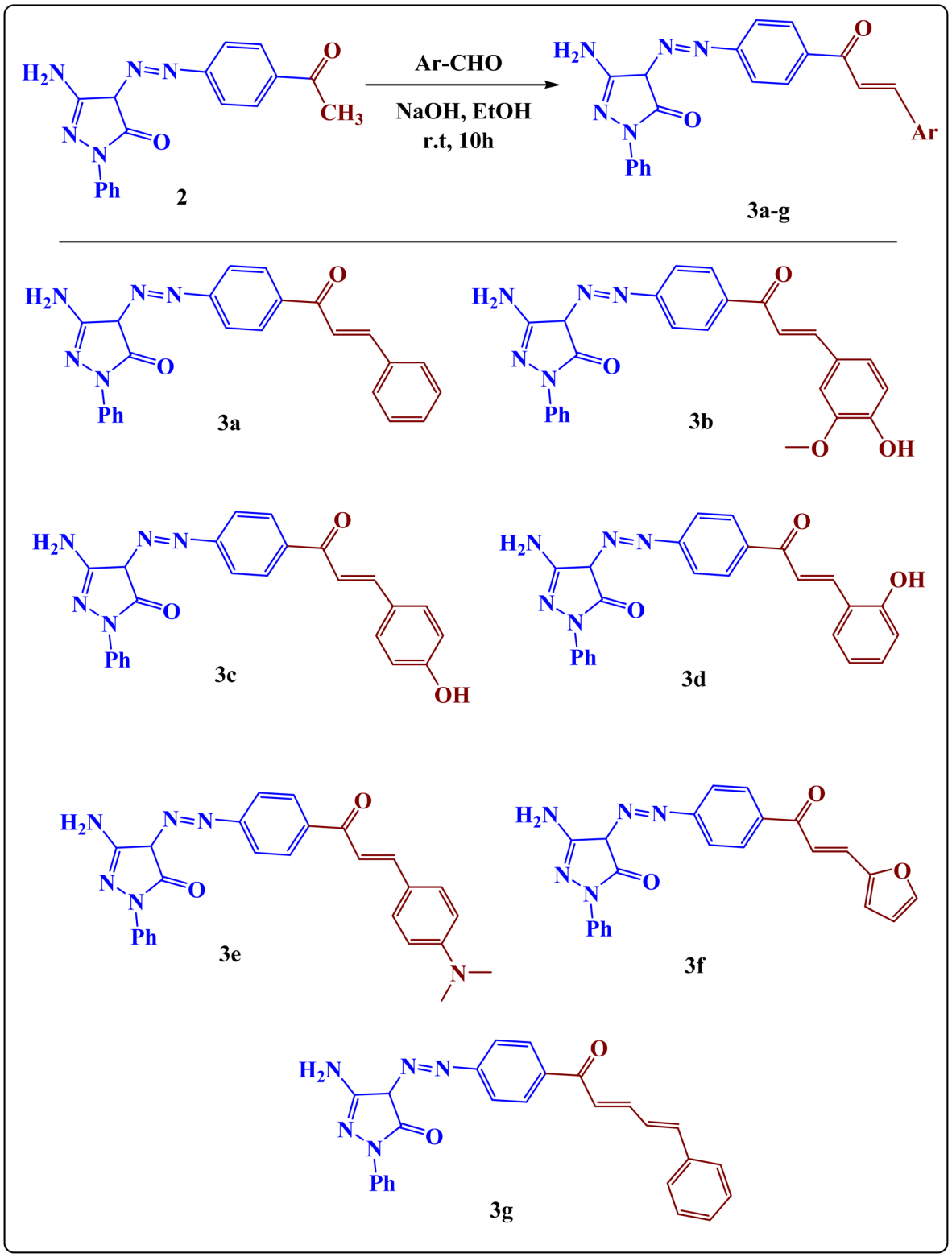

Scheme 2 Synthesis route for compounds **3a–g**.

different absorption bands at 1600 cm^{-1} and 1540 cm^{-1} due to C=O and N=N groups, respectively. Its ^1H NMR spectrum showed a new singlet signal at δ 2.20 ppm attributed to the CH_3 group.

Modifying azo compound (**2**) with a different aromatic aldehyde in a basic medium led to the formation of pyrazolone chalcone **3a–g** (Scheme 2).[24] The FT-IR analysis of chalcones (**3a–g**) showed absorption bands at 1610–1670 cm^{-1}, 1520–1600 cm^{-1}, and 1500–1560 cm^{-1}, for C=O, C=N, and N=N groups. Compound **3b–d** showed absorption bands at 3100–3310 cm^{-1} for the OH group. The ^1H NMR spectrum of compound **3a** revealed two new signals resonated at δ 7.54, and 7.68 ppm attributed to two olefinic protons. Compound **3b** showed four new signals at δ 7.00, 7.40, 3.86, and 2.08 ppm attributed to two olefinic protons, OCH_3 protons, and OH proton, respectively. Additionally, compounds **3c** and **3d** showed three new signals at δ 6.92–7.45, 7.55–7.56, and 10.12–10.26 ppm attributed to two olefinic protons and OH proton, respectively. Finally, the ^1H NMR spectrum of compound **3g** revealed four new signals resonated at δ 7.62, 7.68, 8.02, and 8.07 ppm attributed to olefinic protons.

The suggested mechanism for the synthesis of compounds **3a–g** is illustrated in Scheme 3.

Antioxidant capacity

Fig. 2 and 3 show that the antioxidant activity enhanced with the increase in chalcone concentration using the stable DPPH radical. Compared to normal L-ascorbic acid (IC_{50} = 16.81 ± 0.10 μM), compound **3b** exhibited the greatest DPPH scavenging activity with an IC_{50} value of 19.95 ± 0.14 μM. Compounds **3a** and **3f** exhibited a strong antioxidant activity with IC_{50} values of 21.40 ± 0.17 and 27.25 ± 0.19 μM. Moreover, compounds **3e** and **3d** had moderate effects on scavenging with the activity of 32.79 ± 0.21 and 48.59 ± 0.28 μM, respectively, while compounds **3g** and **3c** showed a limited ability to quench free radicals with IC_{50} values of 73.63 ± 0.39 and 94.18 ± 0.45 μM, respectively.

Docking studies

For creating anticancer drugs, the novel chalcone ligands **3a–g** were docked into YAP/TEAD, a well-known and alluring therapeutic target protein in the Hippo signaling pathway. Numerous studies in the fields of oncology and regenerative medicine have examined the Hippo pathway, and these studies have also suggested that the route may be important as a regulatory variable in human biology or as an inhibitory target for drug

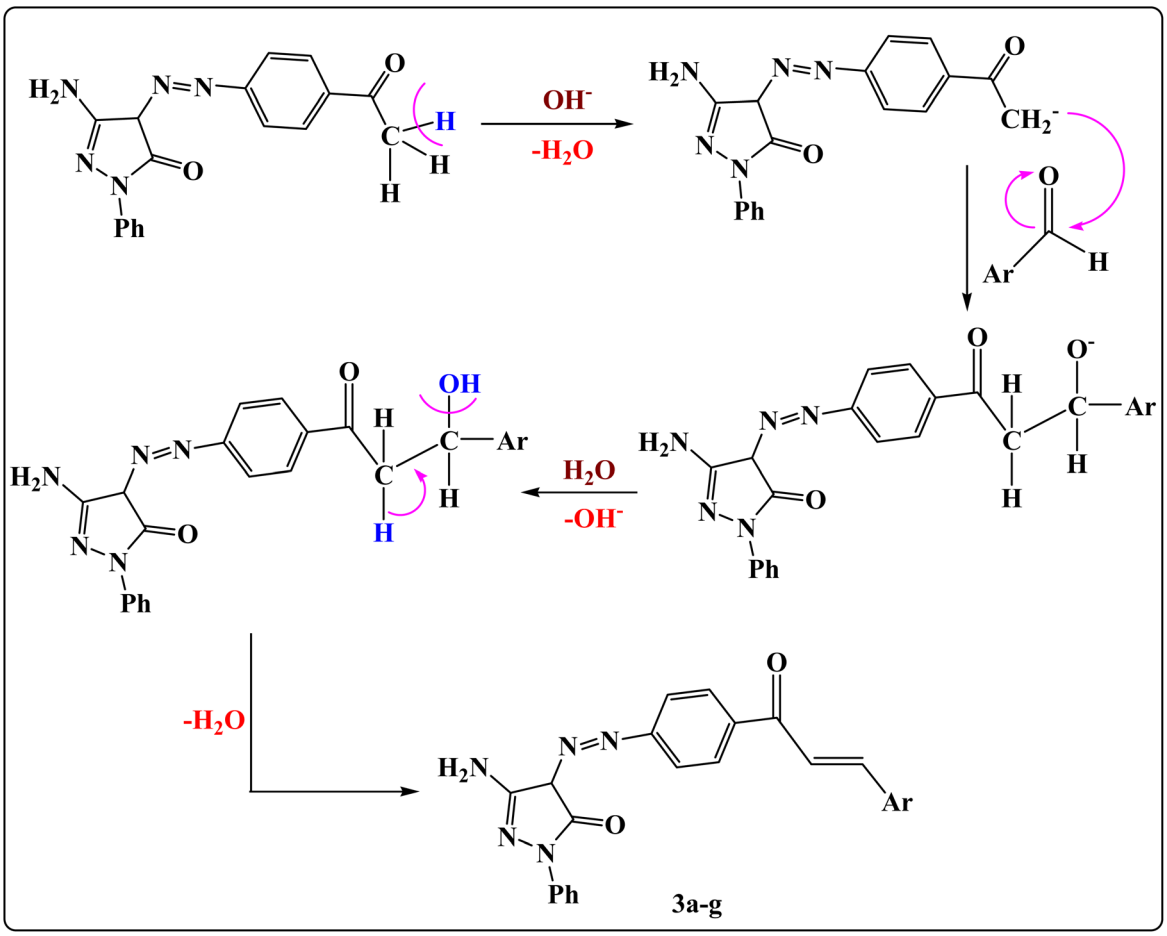

Scheme 3 Suggested mechanism for compounds 3a–g.

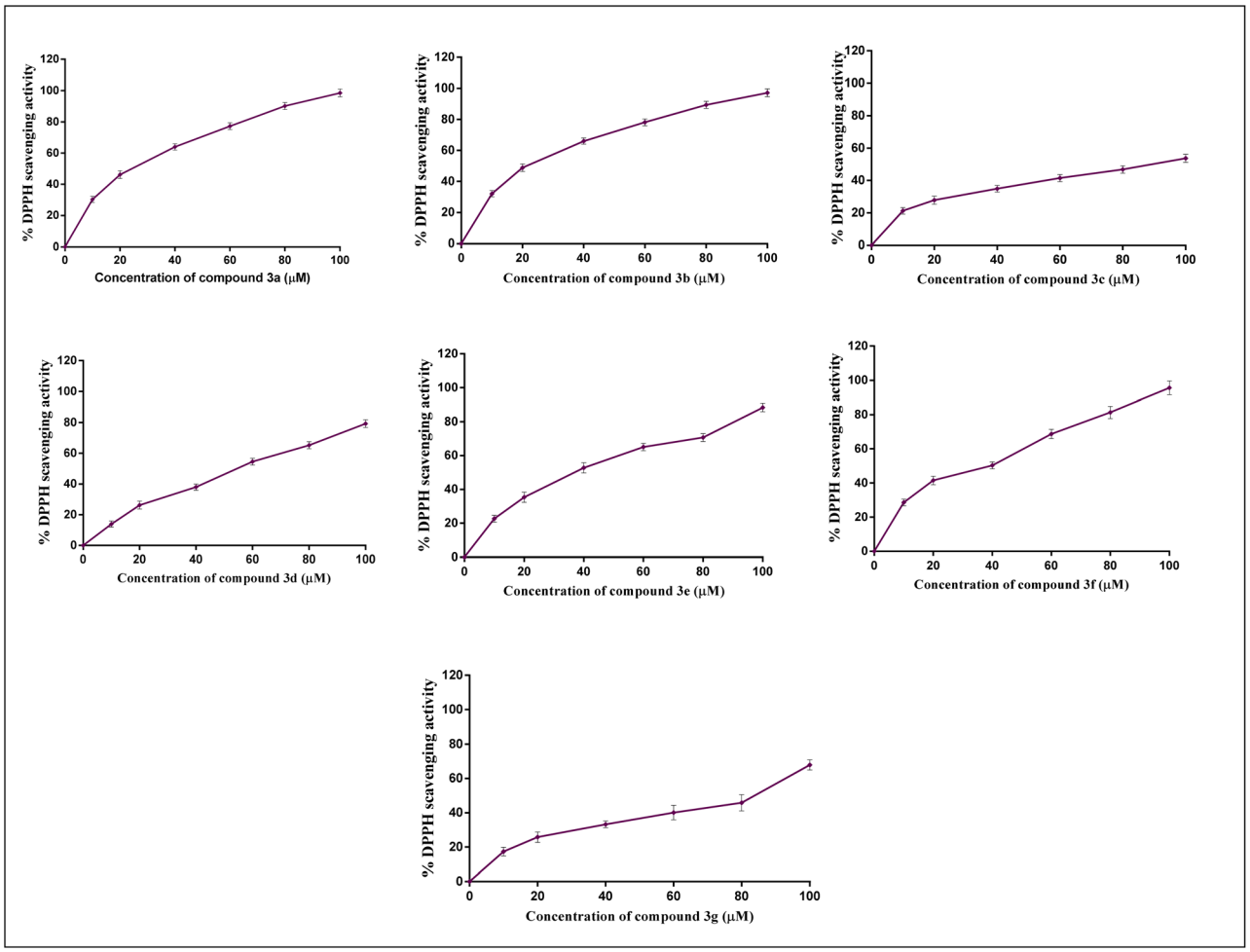

Fig. 2 Antioxidant scavenging activity of chalcone derivatives (**3a–g**). Results are reported as mean ± SE; where $n = 3$.

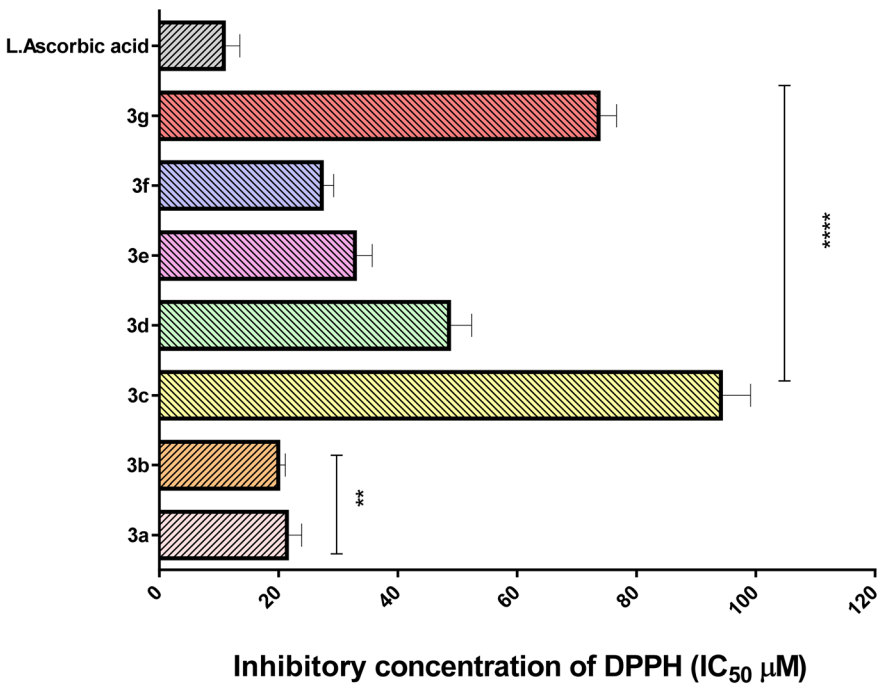

Fig. 3 Inhibitory concentrations (IC_{50}) of chalcones **3a–g** *via* DPPH. Results are reported as mean ± SE, where $n = 3$.

Table 1 Docking scores of compounds **3a–g** with the target protein

Compounds	YAP/TEAD target Hippo signaling protein	
	Docking score (ΔG_{bind})	Docked complex (amino acid–ligand) interactions
3a	−7.86	H-acceptor
		LYS344
		CYS367
		Electrostatic interactions
		PHE229
		LLE395
		MET370
		LEU366
3b	−8.45	H-donor
		PRO365
		π-Hydrogen
		LYS344
		VAL345
		Electrostatic interactions
		LEU366
		MET370
		CYS367
		LLE395
		GLU343
		CYS367
3c	−6.11	Electrostatic interactions
		CYS367
		LEU366
		MET370
		LYS344
		LLE395
3d	−7.11	H-acceptor
		LYS344
		Electrostatic interactions
		CYS367
		THR332
		PHE229
		LLE395
		PHE415
		VAL342
3e	−7.13	H-acceptor
		LYS344
		Electrostatic interactions
		CYS367
		THR332
		PHE229
		LLE395
		PHE415
		VAL342
3f	−7.22	H-acceptor
		LYS344
		Electrostatic interactions
		CYS367
		VAL342
		LLE395
		MET370
		LEU366
3g	−6.09	Electrostatic interactions
		LEU366
		GLU368
		VAL342
		CYS367
		LYS344
		LLE395
		PHE229

development. Generally, the Hippo pathway consists of two constitutive modules: the upstream serine/threonine kinase cascade, which comprises MST1/2 and LATS1/2, and the downstream transcriptional modules, which mainly include the YAP/TEAD complex.[25]

The YAP/TEAD genetic and pharmacological interaction significantly decreased carcinogenesis in YAP-dependent cancer models.[26] As a result, the YAP/TEAD complex has become a desirable target for the creation of anti-cancer medications.[27] Table 1 and Fig. 4 summarize all new chalcone interactions with the target YAP/TEAD protein. According to our findings, compound **3b** had the highest binding energy (−8.45 kcal mol^{-1}) against the target YAP/TEAD protein. Compound **3a** had high binding energy (−7.86 kcal mol^{-1}) with the target protein. With binding energies of −7.11, −7.13, and −7.7.22 kcal mol^{-1}, respectively, compounds **3d**, **3e**, and **3f** also demonstrated a mild inhibitory effect. Conversely, compounds **3c** and **3g** showed low binding energies of −6.11 and −6.09 kcal mol^{-1}, respectively. Compound **3b** was therefore highly recommended for use as an anticancer agent because of its potential to inhibit the YAP/TEAD mediated Hippo signaling pathway.

ADMET features

The bioavailability and drug-like characteristics of the studied chalcone derivatives (**3a–g**) were determined, and are shown in Fig. 5. With a total polar surface area (TPSA) ranging from 102.25 to 149.35 Å^2, the compounds **3a–g** met all the requirements for exceptional permeability and had sufficient oral bioavailability. To further demonstrate flexibility, they also used rotatable bonds between 0 and 10. They were more soluble in cellular membranes because their hydrogen-bond accepted (HBA) and hydrogen-bond donated (HBD) values fell within the fulfilled range. Table 2 demonstrates that octanol/water partition coefficient ($\log p$) values less than 5 were indicative of good lipophilicity features. The chalcone derivatives also showed a higher percentage of human intestinal absorption (HIA) ratings in accordance with the ADMET criteria, indicating that the human intestine could absorb them more effectively. The studied chalcones have a great safety profile for the central nervous system (CNS) since they do not penetrate the blood–brain barrier. They are safe because every AMES toxicity and carcinogenicity test result was negative.

In vitro anticancer study

The antitumor effect of chalcone derivatives (**3a–g**) on HCT-116, HepG2, MCF-7, and WI-38 normal cell lines was assessed in this study using the MTT assay (Fig. 6). Compound **3b** demonstrated noteworthy antitumor effects on the cancer cell lines HepG2, MCF-7, and HCT-116, with IC_{50} values of 5.03 ± 0.4, 3.92 ± 0.2, and 6.34 ± 0.5 μM, respectively. Compounds **3a** and **3f** demonstrated impressive antitumor effects with HCT-116, HepG2, and MCF-7 cell lines. Compounds **3e** and **3d** demonstrated a moderate effect on all cancer cell lines. Conversely, Compounds **3g** and **3c** demonstrated a weak effect

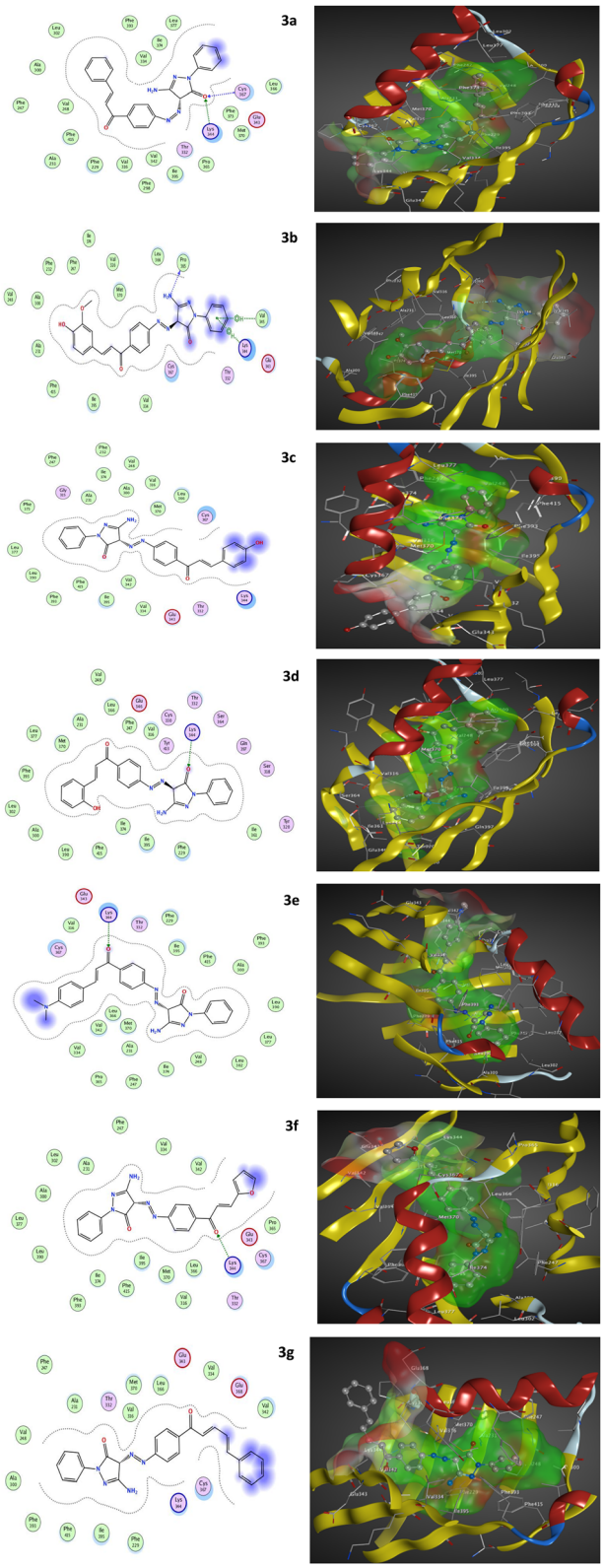

Fig. 4 Two- and three-dimensional molecular interaction networks for all chalcone derivatives (**3a–g**) with the target YAP/TEAD-mediated Hippo signaling pathway.

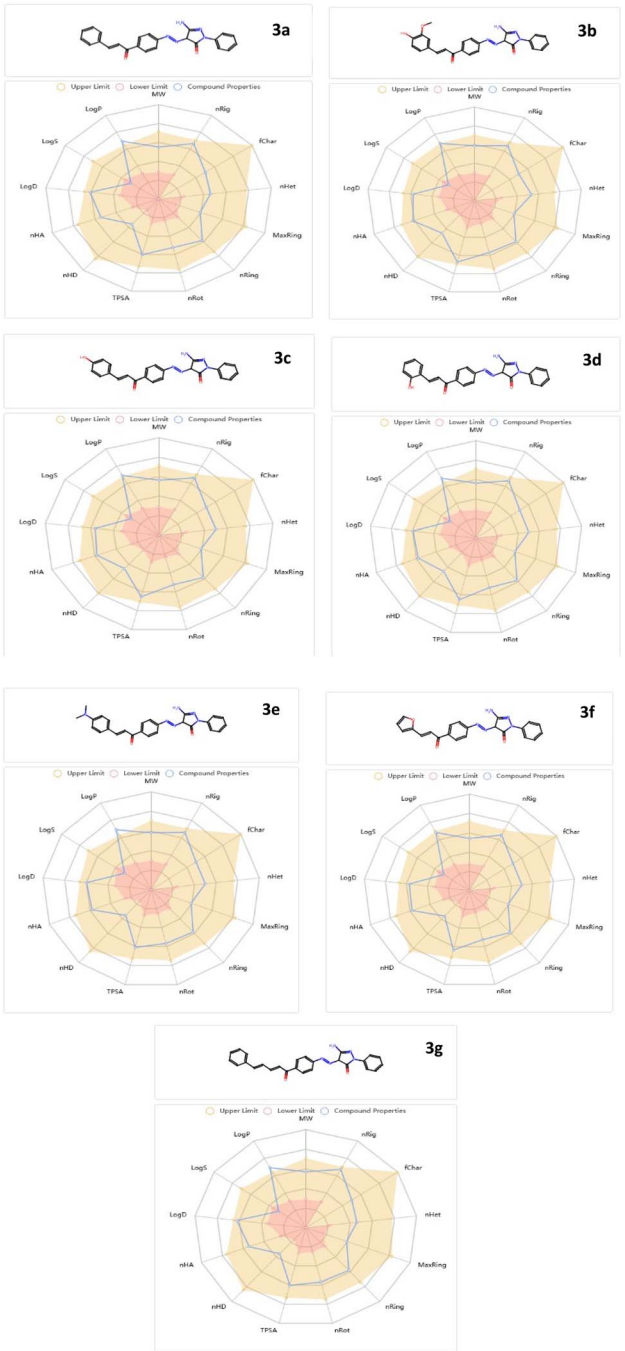

Fig. 5 Bioavailability radar plot for chalcones (**3a–g**).

on all cancer cell lines when compared to the reference chemotherapeutic drug (DOX). Moreover, all new derivatives (**3a–g**) showed lower cytotoxic effects on WI-38 normal cells except **3c**. Our finding was in line with the previous study.[24] This suggests that compound **3b** worked against proliferative cancer by blocking the Hippo signaling pathway mediated by YAP/TEAD.

Table 2 ADMET assets

	Molecular weight (g mol^{-1})	Blood–brain barrier (BBB)	% human intestinal absorption (HIA+)	TPSA A^2	log p	nHA	nHD	N rotatable	AMES toxicity	Carcinogenicity
3a	409.15	No	89.6	100.48	3.39	7	2	6	Nontoxic	Noncarcinogenic
3b	455.16	No	92.1	129.94	2.98	9	3	7	Nontoxic	Noncarcinogenic
3c	425.15	No	84.3	120.71	3.08	8	3	6	Nontoxic	Noncarcinogenic
3d	425.15	No	75.9	120.71	3.43	8	3	6	Nontoxic	Noncarcinogenic
3e	452.20	No	83.4	103.72	3.61	8	2	7	Nontoxic	Noncarcinogenic
3f	399.13	No	79.1	113.62	2.90	8	2	6	Nontoxic	Noncarcinogenic
3g	435.17	No	77.3	100.48	3.47	7	2	7	Nontoxic	Noncarcinogenic

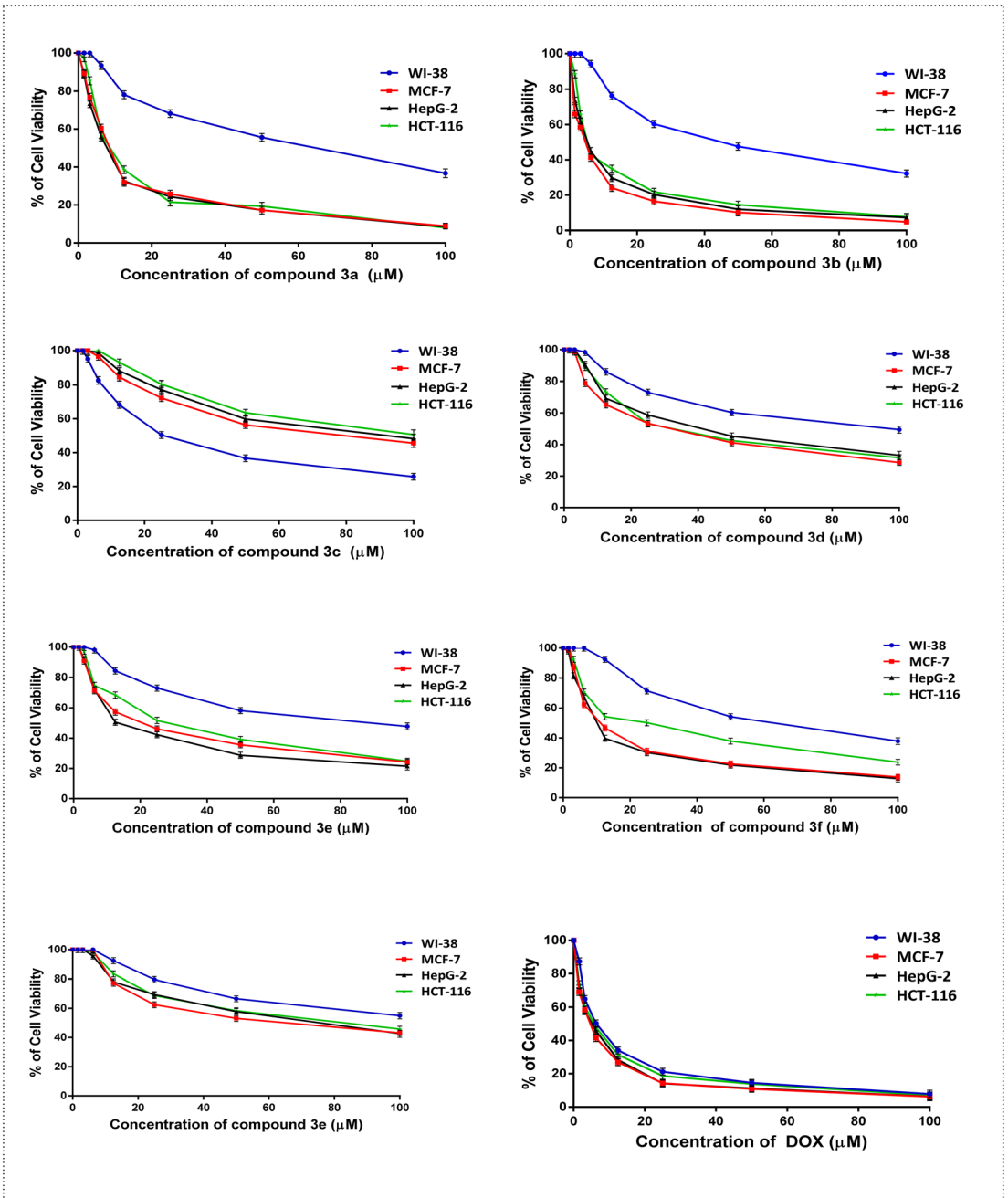

Fig. 6 Antitumor and cytotoxic impacts of chalcones **3a–g**. Results are reported as mean ± SE of three independent triplicates.

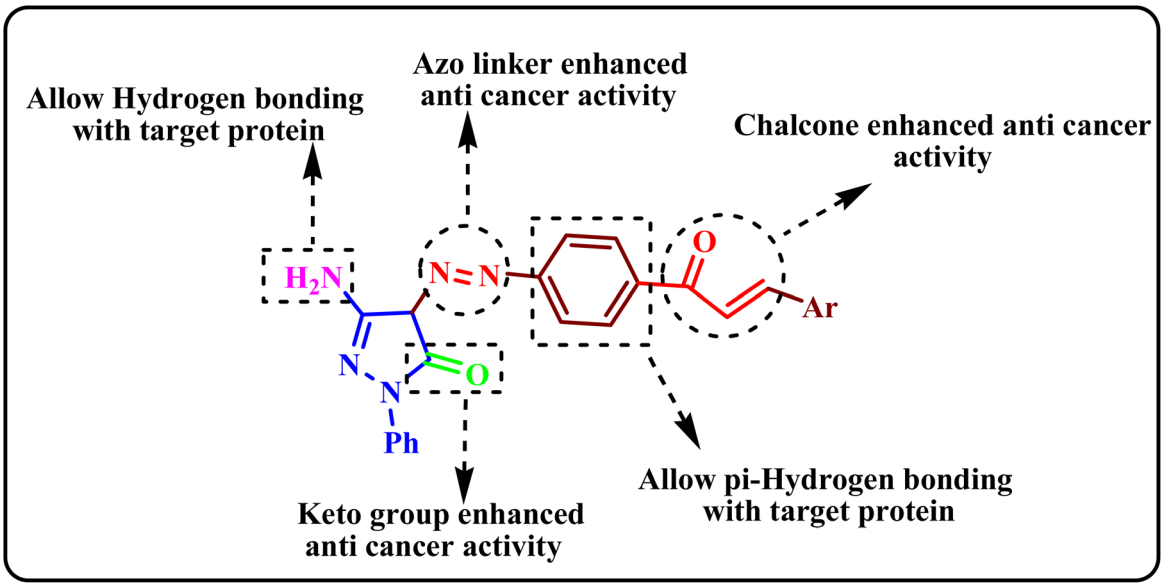

Fig. 7 SAR of the most active compound.

Structure–anti-tumor activity relationship (SAR)

The synthesized chalcones demonstrated their anticancer effect for the following reasons (Fig. 7):

- The presence of different substituents in the aryl group enhanced cytotoxic activity against different cancer cell lines (HepG-2, MCF-7, and HCT-116).
- The presence of hetero atoms such as nitrogen as well as carbonyl groups in the chemical structure of the pyrazolone chalcones enhanced the value of binding energy through the interaction between the pyrazolone chalcone and the target protein *via* hydrogen bonding.[28]
- The azo linker enhanced the hydrogen bonding with the target protein 29.
- Compound **3b** was considered the most active compound due to the presence of the phenyl group and olefinic protons, which enhanced the hydrogen bonding and π–π interaction with the target protein and, hence, increased the value of the binding energy.[30]

Conclusion

We synthesized and characterized new pyrazolone chalcones (**3a–g**) using various spectral data. Among all the synthesized compounds, chalcone **3b** demonstrated the strongest antioxidant activity. Furthermore, it has a high docking score because of hydrogen bonds, hydrophobic interactions, and electrostatic interactions with important residues in the binding pocket of the YAP/TEAD target protein. For that, molecular docking suggested that it may be a targeted anticancer agent. Additionally, the *in vitro* anti-cancer effect against different cancer cell lines was explained by the suppressive effect of chalcone **3b**, which inhibited the YAP/TEAD-mediated Hippo signaling pathway to cause apoptosis and obstruct cell growth and survival. According to these results, chalcone **3b** may be a newly targeted anticancer scaffold that targets a variety of cancer cells.

Experimental section

Materials and instrumentation

Section S1 in the ESI† includes the data of chemicals and instrumentation.

Synthesis of 3-amino-1-phenyl-1*H*-pyrazol-5(4*H*)-one (1)

Weissberger lab was previously preparing compound **1** (ref. 23)

Synthesis of 4-((4-acetylphenyl)diazenyl)-3-amino-1-phenyl-1*H*-pyrazol-5(4*H*)-one (2)

A sodium nitrite solution (12.7 mmol) was added slowly to *p*-amino acetophenone (13.7 mmol) in concentrated HCl. The resulting diazonium chloride was added to a solution of compound **1** (8.5 mmol) in pyridine. Then, the product was filtered and dried.

Orange powder; yield 74%; mp 89–91 °C; ^{1}H NMR (400 MHz, DMSO-d_6) δ (ppm): 9.14 (s, 2H, NH_2), 7.08–8.11 (m, 9H, Ar–H), 2.59 (s, 1H, CH–pyrazolone), 2.20 (s, 3H, CH_3); IR (KBr) ν: 1600 (CO), 1540 (N=N); anal. calcd for $C_{17}H_{15}N_5O_2$ (321.33): C, 63.54%; H, 4.71%; N, 21.79%. Found: C, 63.34%; H, 4.57%; N, 21.67%.

General procedure for the synthesis of pyrazolone chalcones (3a–g)

An ethanolic solution of compound **2** (10.0 mmol), aromatic aldehyde (10.0 mmol), and sodium hydroxide (20.0 mmol) was stirred at 25 °C for 10 h, put into freezing water, filtered, and then dried.

5-Amino-4-((*E*)-(4-cinnamoylphenyl)diazenyl)-2-phenyl-2,4-dihydro-3*H*-pyrazol-3-one (3a). Orange powder; yield 76%; mp 228–230 °C; ^{1}H NMR (400 MHz, DMSO-d_6) δ (ppm): 10.55 (s, 2H, NH_2), 7.68 (d, 1H, =CH), 7.54 (d, 1H, COCH=), 6.54–8.40 (m, 14H, Ar–H), 2.60 (s, 1H, CH–pyrazolone); ^{13}C NMR (101 MHz, DMSO-d_6) δ (ppm): 171.72 (C=O chalcone), 168.04 (C=O

pyrazolone), 146.95 (C=N pyrazolone), 113.20–133.22 (Ar–C), 127.60, 135.25 (C–olefinic), 74.43 (CH–pyrazolone); IR (KBr) ν: 3405 (NH_2), 1650 (C=O), 1597 (C=N), 1550 (N=N); anal. calcd for $C_{24}H_{19}N_5O_2$ (409.15): C, 70.40%; H, 4.68%; N, 17.10%. Found: C, 70.25%; H, 4.46%; N, 17.02%.

5-Amino-4-((*E*)-(4-((*E*)-3-(4-hydroxy-3-methoxyphenyl) acryloyl)phenyl)diazenyl)-2-phenyl-2,4-dihydro-3*H*-pyrazol-3-one (3b). Orange powder; yield 84%; mp 103–105 °C; ^{1}H NMR (400 MHz, DMSO-d_6) δ (ppm): 9.76 (s, 2H, NH_2), 7.40 (d, 1H, =CH), 7.00 (d, 1H, COCH=), 6.89–8.17 (m, 12H, Ar–H), 3.86 (s, 3H, OCH_3), 2.61 (s, 1H, CH–pyrazolone), 2.08 (s, 1H, OH); ^{13}C NMR (101 MHz, DMSO-d_6) δ (ppm):153.80 (C=O chalcone), 150.94 (C=O pyrazolone), 149.03 (C=N pyrazolone), 145.49 (C–OH), 111.54–130.62 (Ar–C), 122.71, 130.93 (C–olefinic), 70.29 (CH–pyrazolone), 55.98 (OCH_3); IR (KBr) ν: 3400 (NH_2), 3310 (OH), 1610 (C=O), 1600 (C=N), 1520(N=N); anal. calcd for $C_{25}H_{21}N_5O_4$ (455.16): C, 65.93%; H, 4.65%; N, 15.38%. Found: C, 65.77%; H, 4.47%; N, 15.26%.

5-Amino-4-((*E*)-(4-((*E*)-3-(4-hydroxyphenyl)acryloyl)phenyl) diazenyl)-2-phenyl-2,4-dihydro-3*H*-pyrazol-3-one (3c). Brownish orange powder; yield 83%; mp 148–150 °C; ^{1}H NMR (400 MHz, DMSO-d_6) δ (ppm): 10.12 (s, 1H, OH), 9.79 (s, 2H, NH_2), 7.56 (d, 1H, =CH), 6.92 (d, 1H, COCH=), 6.84–8.21 (m, 13H, Ar–H), 2.59 (s, 1H, CH–pyrazolone); ^{13}C NMR (101 MHz, DMSO-d_6) δ (ppm):163.65 (C=O chalcone), 160.64 (C=O pyrazolone), 159.35 (C=N pyrazolone), 135.57 (C–OH), 98.54–131.58 (Ar–C), 123.23, 132.56 (C–olefinic), 74.42 (CH–pyrazolone); IR (KBr) ν: 3400 (NH_2), 3200 (OH), 1620 (C=O), 1590 (C=N), 1520(N=N); anal. calcd for $C_{24}H_{19}N_5O_3$ (425.15): C, 67.76%; H, 4.50%; N, 16.46%. Found: C, 67.66%; H, 4.36%; N, 16.38%.

5-Amino-4-((*E*)-(4-((*E*)-3-(2-hydroxyphenyl)acryloyl)phenyl) diazenyl)-2-phenyl-2,4-dihydro-3*H*-pyrazol-3-one (3d). Orange powder; yield 84%; mp 143–145 °C; ^{1}H NMR (400 MHz, DMSO-d_6) δ (ppm): 10.26 (s, 1H, OH), 9.79 (s, 2H, NH_2), 7.55 (d, 1H, =CH), 7.45 (d, 1H, COCH=), 6.79–8.22 (m, 13H, Ar–H), 2.60 (s, 1H, CH–pyrazolone); ^{13}C NMR (101 MHz, DMSO-d_6) δ (ppm): 167.74 (C=O chalcone), 156.32 (C=O pyrazolone), 146.51 (C=N pyrazolone), 143.65 (C–OH), 116.98–131.27 (Ar–C), 122.70, 133.51 (C–olefinic), 63.92 (CH–pyrazolone); IR (KBr) ν: 3200 (NH_2), 3100 (OH), 1670 (C=O), 1600 (C=N), 1540 (N=N); anal. calcd for $C_{24}H_{19}N_5O_3$ (425.15): C, 67.76%; H, 4.50%; N, 16.46%. Found: C, 67.66%; H, 4.42%; N, 16.38%.

5-Amino-4-((*Z*)-(4-((*E*)-3-(4-(dimethylamino)phenyl)acryloyl) phenyl)diazenyl)-2-phenyl-2,4-dihydro-3*H*-pyrazol-3-one (3e). Dark brown powder; yield 81%; mp 112–114 °C; ^{1}H NMR (400 MHz, DMSO-d_6) δ (ppm): 9.67 (s, 2H, NH_2), 7.55 (d, 1H, =CH), 6.74 (d, 1H, COCH=), 7.09–8.35 (m, 13H, Ar–H), 3.04 (s, 6H, $N(CH_3)_2$), 2.84 (s, 1H, CH–pyrazolone); ^{13}C NMR (101 MHz, DMSO-d_6) δ (ppm):154.73 (C=O chalcone), 152.51 (C=O pyrazolone), 145.51 (C=N pyrazolone), 111.52–137.28 (Ar–C), 122.98, 138.22 (C–olefinic), 79.78 (CH–pyrazolone), 55.34 ($N(CH_3)_2$); IR (KBr) ν: 3400 (NH_2), 1660 (C=O), 1520 (C=N), 1500 (N=N); anal. calcd for $C_{26}H_{24}N_6O_2$ (452.20): C, 69.01%; H, 5.35%; N, 18.57%. Found: C, 68.91%; H, 5.55%; N, 18.39%.

(*E*)-3-Amino-4-((4-(3-(furan-2-yl)acryloyl)phenyl)diazenyl)-1-phenyl-1*H*-pyrazol-5(4*H*)-one (3f). Black powder; yield 79%; mp 165–167 °C; ^{1}H NMR (400 MHz, DMSO-d_6) δ (ppm): 9.91 (s, 2H, NH_2), 7.92 (d, 1H, =CH), 7.13 (d, 1H, COCH=), 6.71–8.17 (m, 12H, Ar–H), 2.17 (s, 1H, CH–pyrazolone); ^{13}C NMR (101 MHz, DMSO-d_6) δ (ppm): 151.58 (C=O chalcone), 147.45 (C=O pyrazolone), 146.80 (C=N pyrazolone), 112.83–136.01 (Ar–C), 124.28, 136.37 (C–olefinic), 75.72 (CH–pyrazolone); IR (KBr) ν: 3420 (NH_2), 1630 (C=O), 1600 (C=N), 1530 (N=N); anal. calcd for $C_{22}H_{17}N_5O_3$ (399.13): C, 66.16%; H, 4.29%; N, 17.53%. Found: C, 66.06%; H, 4.21%; N, 17.35%.

5-Amino-2-phenyl-4-((*E*)-(4-((2*E*,4*E*)-5-phenylpenta-2,4-dienoyl)phenyl)diazenyl)-2,4-dihydro-3*H*-pyrazol-3-one (3g). Brown powder; yield 83%; mp 152–154 °C; ^{1}H NMR (400 MHz, DMSO-d_6) δ (ppm): 6.39 (s, 2H, NH_2), 8.07 (t, 1H, =CH–CH), 8.02 (d, 1H, COCH=), 7.68 (t, 1H, CH=CH–Ar), 7.62 (d, 1H, CH=CH–Ar), 6.74–8.60 (m, 14H, Ar–H), 2.08 (s, 1H, CH–pyrazolone); IR (KBr) ν: 3400 (NH_2), 1620 (C=O), 1590 (C=N), 1560 (N=N); anal. calcd for $C_{26}H_{21}N_5O_2$ (435.17): C, 71.71%; H, 4.86%; N, 16.08%. Found: C, 71.55%; H, 4.68%; N, 15.92%.

Biological investigations

Antioxidant activity using DPPH. Using a modified Zheleva-Dimitrova approach, the synthesized chalcone derivatives' ability to scavenge free radicals [DPPH] was evaluated.[31,32]

Docking and ADMET *in silico* studies. The pyrazolone chalcones' binding processes to the target protein YAP/TEAD were assessed by the molecular docking experiment.[33,34] To estimate the ADMET features, the web tool Swiss ADME was used. The ESI, Section S2,† has comprehensive details.

Anticancer assessments (*in vitro*)

MTT assay. A panel of cell lines, namely MCF-7, HCT-116, HepG-2, and WI-38 (human lung fibroblast), was used to identify the anticancer activity of pyrazolone chalcones (**3a–g**). El-Nahass described the experimental details.[35]

Statistical analysis. The statistical analysis was performed using GraphPad Prism 6 (San Diego, CA) (GraphPad Prism 6, https://www.graphpad.com/scientific-software/prism/).

Abbreviations

FT-IR	Fourier transform infrared
NMR	nuclear magnetic resonance
DPPH	2,2-diphenyl-1-picrylhydrazyl
ADMET	absorption–distribution–metabolism–excretion–toxicity
HBA	hydrogen bond accepted
HBD	hydrogen bond donated
HIA	human intestinal absorption
CNS	central nervous system
log *P*	octanol/water partition coefficient

Data availability

The cell lines were provided by the American Type Culture Collection (ATCC) *via* VACSERA, Cairo, Egypt, and all accession codes were added: mammary gland (MCF-7; #ATCC HTB-22 (https://www.atcc.org/products/htb-22)), colorectal

adenocarcinoma (HCT-116; #ATCC CCL-247 (**https://www.atcc.org/products/htb-37**)), hepatocellular carcinoma (HepG-2; #ATCC HB-8065 (**https://www.atcc.org/products/hb-8065**)), and human lung fibroblast (WI-38; #ATCC CCL-75 (**https://www.atcc.org/products/ccl-75**)). The datasets used and/or analyzed during the current study are available from the corresponding author on reasonable request. The macromolecule protein structure is deposited in the world-wide protein data bank repository (**https://www.rcsb.org/structure/3KYS**).

Author contributions

Ahmed A. Noser, Maha M. Salem, and Esraa M. ElSafty: writing – review & editing, writing – original draft, and methodology. Maha M. Salem: formal analysis. Adel I. Selim, Ahmed A. Noser, Mohamed H. Baren, and Hamada S. A. Mandour: supervision.

Conflicts of interest

The authors have no relevant financial or non-financial interests to disclose.

References

1 P. Das, G. Sayan, A. Tarun, M. Pritiprasanna, G. Sabyasachi, C. Sumita and G. Subhashis, *Mater. Chem. Phys.*, 2019, **237**, 121860.
2 W. Cao, H. D. Chen, Y. W. Yu, N. Li and W. Q. Chen, *Chin. Med.*, 2020, **134**, 783e791.
3 L. Zhang, F. Ren, Q. Zhang, Y. Chen, B. Wang and J. Jiang, *Dev. Cell*, 2008, **14**, 377–387.
4 Y. Zhao and X. Yang, *Int. J. Cancer*, 2015, **137**, 2767–2773.
5 J. V. Patil, S. S. Shubhangi, U. Shweta, G. Pankaj and B. Suresh, *ChemistrySelect*, 2024, **9**, e202303391.
6 S. M. Emam, B. Samir and A. M. Ahmed, *Results Chem.*, 2023, **5**, 100725.
7 A. N. Ahmed, H. A. Aboubakr and M. S. Maha, *Bioorg. Chem.*, 2023, **131**, 106299.
8 A. N. Ahmed, A. S. Ihsan, H. A. Aboubakr and M. S. Maha, *ACS Omega*, 2022, **7**, 25265–25277.
9 M. Islam, M. Abdullah, N. Essam, Y. Sammer, A. Muhammad, N. Asif and W. Abdul, *J. Mol. Struct.*, 2022, **1269**, 133843.
10 S. Dabhade, P. Manjushri, S. Lala, A. Sachin, A. Shweta, Y. Somdatta and N. Santosh, *Chem. Biodiversity*, 2024, **21**, e202400015.
11 F. Rizk, N. Ahmed, A. Seham and K. Amira, *J. Heterocycl. Chem.*, 2022, **59**, 2190–2206.
12 H. Şenol, G. Mansour, Ö. Gülbahar, T. Alim and G. Uğur, *J. Mol. Struct.*, 2024, **1295**, 136804.
13 A. N. Ahmed, A. A. El-Barbary, M. S. Maha, A. Hayam and S. Mohamed, *Sci. Rep.*, 2024, **14**, 3530.
14 K. J. Setshedi, M. B. Richard, I. Kayhan, M. Dorien, C. Guy and J. L. Lesetja, *Med. Chem. Res.*, 2024, **3**, 977–988.
15 A. N. Ahmed, A. I. Saham, A. Hayam, M. A. Nora and S. A. Hamada, *J. Iran. Chem. Soc.*, 2023, **20**, 2963–2976.
16 S. S. Shafi, *Indian J. Chem., Sect. B: Org. Chem. Incl. Med. Chem.*, 2021, **60**, 1132–1136.
17 S. K. Ramadan and A. R. Sameh, *J. Iran. Chem. Soc.*, 2022, **19**, 187–201.
18 J. Zhou, W. Feng, X. Bin, L. Xin, P. Cheng and F. U. Peng, *Oncol. Res.*, 2024, **32**, 943.
19 H. Tanaka, N. Seito, O. Kenji, T. Tomoya and H. Toshihiko, *Biochem. Biophys. Res. Commun.*, 2009, **381**, 566–571.
20 G. Padmavathi, K. R. Nand, B. Devivasha, A. Frank, M. Srishti, S. Gautam, B. Anupam and B. K. Ajaikumar, *Phytomedicine*, 2017, **25**, 118–127.
21 A. Jasiecka, T. Maslanka and J. J. Jaroszewski, *Pol. J. Vet. Sci.*, 2014, **17**, 207–214.
22 H. G. Kraetsch, T. Hummel, J. Lötsch, R. Kussat and G. Kobal, *Eur. J. Clin. Pharmacol.*, 1996, **49**, 377–382.
23 A. Weissberger, H. D. Porter and W. A. Gregory, *J. Am. Chem. Soc.*, 1944, **66**, 1851–1855.
24 J. Dong, H. Guang, Z. Qijing, W. Zengtao, C. Jiahua, W. Yan, M. Qingqing and L. Shaoshun, *MedChemComm*, 2019, **10**, 1606–1614.
25 B. Zhao, X. Ye, J. Yu, L. Li, W. Li, S. Li, J. Yu, J. D. Lin, C. Y. Wang, A. M. Chinnaiyan, Z. C. Lai and K. L. Guan, *Genes Dev.*, 2008, **22**, 1962–1971.
26 Y. Liu-Chittenden, B. Huang, J. S. Shim, Q. Chen, S. J. Lee, R. A. Anders, J. O. Liu and D. Pan, *Genes Dev.*, 2012, **26**, 1300–1305.
27 H. Zhang, S. K. Ramakrishnan, D. Triner, B. Centofanti, D. Maitra, B. Gyorffy, J. S. Sebolt-leopold, M. K. Dame, J. Varani, D. E. Brenner, E. R. Fearon, M. B. Omary and Y. M. Shah, *Sci. Signaling*, 2015, **8**, 98.
28 A. N. Ahmed, E. Mohamed, D. Thoria and H. A. Aboubakr, *Molecules*, 2020, **25**, 4780.
29 S. K. Liew, M. Sharan, M. A. Norhafiza and H. N. Noor, *Biomolecules*, 2020, **10**, 138.
30 Y. Ali, S. A. Hamid and R. Umer, *Mini-Rev. Med. Chem.*, 2018, **18**, 1548–1558.
31 W. M. Hamada, M. N. El-Nahass, A. A. Noser, T. A. Fayed, M. El-Kemary, M. M. Salem and E. Bakr, *Sci. Rep.*, 2023, **13**, 15420.
32 A. Noser, H. Mohamed, A. Saham, M. Rekaby and M. Maha, *ChemistrySelect*, 2023, **8**, e202204670.
33 Y. Son, J. Kim, Y. Kim, S. G. Chi, T. Kim and J. Yu, *Bioorg. Chem.*, 2023, **131**, 106274.
34 H. A. Hekal, O. M. Hammad, N. R. El-Brollosy, M. M. Salem and A. K. Allayeh, *Bioorg. Chem.*, 2024, **147**, 107353.
35 M. N. El-Nahass, E. A. Bakr, T. A. Fayed, W. M. Hamada, M. M. Salem and A. M. Radwan, *J. Iran. Chem. Soc.*, 2024, **21**, 699–718.